THE GEOLOGICAL SOCIETY OF AMERICA®

A volcanic trigger for the Late Ordovician mass extinction? Mercury data from south China and Laurentia

David S. Jones[1], Anna M. Martini[1], David A. Fike[2], and Kunio Kaiho[3]
[1]Amherst College Geology Department, 11 Barrett Hill Road, Amherst, Massachusetts 01002, USA
[2]Department of Earth and Planetary Sciences, Washington University in Saint Louis, 1 Brookings Drive, Saint Louis, Missouri 63130, USA
[3]Department of Earth Science, Tohoku University, 6-3 Aramaki-aza aoba, Aoba-ku, Sendai 980-8578, Japan

ABSTRACT

The Late Ordovician mass extinction (LOME), one of the five largest Phanerozoic biodiversity depletions, occurred in two pulses associated with the expansion and contraction of ice sheets on Gondwana during the Hirnantian Age. It is widely recognized that environmental disruptions associated with changing glacial conditions contributed to the extinctions, but neither the kill mechanisms nor the causes of glacial expansion are well understood. Here we report anomalously high Hg concentrations in marine strata from south China and Laurentia deposited immediately before, during, and after the Hirnantian glacial maximum that we interpret to reflect the emplacement of a large igneous province (LIP). An initial Hg enrichment occurs in the late Katian Age, while a second enrichment occurs immediately below the Katian-Hirnantian boundary, which marks the first pulse of extinction. Further Hg enrichment occurs in strata deposited during glacioeustatic sea-level fall and the glacial maximum. We propose that these Hg enrichments are products of multiple phases of LIP volcanism. While elevated Hg concentrations have been linked to LIP emplacement coincident with other Phanerozoic mass extinctions, the climate response during the LOME may have been unique owing to different climatic boundary conditions, including preexisting ice sheets. Our observations support a volcanic trigger for the LOME and further point to LIP volcanism as a primary driver of environmental changes that caused mass extinctions.

INTRODUCTION

Paleoclimate records indicate global cooling during ~35 m.y. of the Early and Middle Ordovician, a relatively stable climate in the ~8-m.y.-long Katian Age, and a glacial maximum in the Hirnantian Age (445.2–443.8 Ma) (Trotter et al., 2008; Finnegan et al., 2011; Melchin et al., 2013). Cooling likely resulted in the establishment of ice sheets on polar Gondwana in the Katian Age or even earlier (Saltzman and Young, 2005; Finnegan et al., 2011; Pohl et al., 2016). The subsequent rapid expansion of Hirnantian ice sheets resulted in glacioeustatic sea-level fall and decreased temperatures (Finnegan et al., 2011) associated with the first pulse of the Late Ordovician mass extinction (LOME) (Melchin et al., 2013). The second pulse of the LOME occurred as glaciers melted, oceans warmed, and anoxic seawater transgressed the shelves (Melchin et al., 2013). The cause of the glacial advance is unknown, but has been attributed to CO_2 levels falling below a critical threshold (Herrmann et al., 2004). Lefebvre et al. (2010) used a coupled biogeochemical-energy balance model to demonstrate that chemical weathering of a hypothetical late Katian large igneous province (LIP) could have lowered CO_2 over millions of years to cause major ice sheet growth. However, geological and geochemical evidence of such an eruption are currently lacking, and it is unclear if the apparent rapid time scale of the Hirnantian glacial advance is consistent with a weathering mechanism.

Phanerozoic mass extinctions have been linked geochronologically and mechanistically to the emplacement of LIPs (Courtillot and Renne, 2003; Bond and Wignall, 2014). CO_2 release associated with LIP emplacement can produce greenhouse warming, ocean acidification, and marine anoxia (Self et al., 2014), and SO_2 release can induce short-term cooling through the production of stratospheric sulfur aerosols (Schmidt et al., 2015). Volcanism is the major preanthropogenic source of mercury to Earth's surface environments (Selin, 2009), and the accumulation of Hg in sediment can be used as a proxy for ancient volcanic events (Sanei et al., 2012; Font et al., 2016; Thibodeau et al., 2016). The atmospheric residence time of Hg is long (~1–2 yr) (Selin, 2009) relative to atmospheric mixing time, and volcanogenic Hg can accumulate globally (Schuster et al., 2002). Because Hg binds to organic matter in marine settings, Hg concentration per unit of total organic carbon (TOC) is a useful measure of environmental Hg loading in modern (Fitzgerald et al., 2007) and ancient (Sanei et al., 2012) environments. Hg and Hg/TOC enrichments are observed in marine strata deposited during Phanerozoic mass extinctions associated with known LIPs, including the Siberian Traps at the Permian-Triassic boundary (Sanei et al., 2012), the Central Atlantic magmatic province at the Triassic-Jurassic boundary (Thibodeau et al., 2016), and the Deccan Traps at the Cretaceous-Paleogene boundary (Font et al., 2016).

GEOLOGIC SETTING AND METHODS

In order to develop records of Hg loading associated with the LOME, we analyzed samples from successions in south China and Laurentia spanning the interval of the LOME and Hirnantian glacial maximum (Fig. 1).

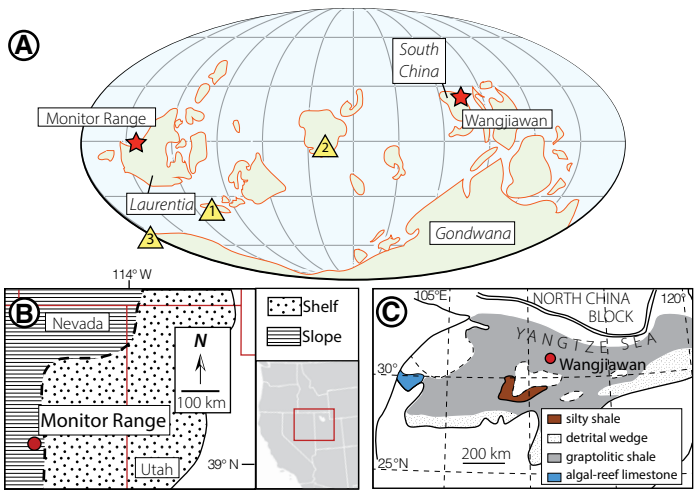

Figure 1. Late Ordovician paleogeography and study locations. A: Paleogeographic reconstruction at 446 Ma, modified from Kilian et al. (2016). Stars mark locations of stratigraphic sections at the Monitor Range (western Laurentia; Nevada, USA) and Wangjiawan (south China). Triangles mark the locations of Late Ordovician mafic provinces: 1—Cape St. Mary's sills, Newfoundland; 2—Suordakh, Siberia; 3—Sierra del Tigre, Argentina. B: Location map for the Monitor Range (after Jones et al., 2016). C: Location map for Wangjiawan (after Gorjan et al., 2012).

At Wangjiawan in south China, dark shale of the Wufeng Formation was deposited on an anoxic deep shelf facing the open ocean (Chen et al., 2006) (Fig. 2A). The overlying shaley limestone of the Kuanyinchiao Formation was deposited during shallowing; these strata represent the transition to cool-water carbonate deposition and host the *Hirnantia* fauna characteristic of the glacial maximum (Chen et al., 2006). The overlying Lungamachi Formation represents postglacial flooding of the basin (Chen et al., 2006). At the Monitor Range (Nevada, USA) of western Laurentia, the lower Hanson Creek Formation consists of dark lime mudstone deposited below wave base; limestone of the upper Hanson Creek Formation was deposited in progressively shallower environments with an exposure surface succeeded by deepening at the top of the succession (Finney et al., 1997) (Fig. 2B). Both successions contain the globally recognized Hirnantian positive carbon isotope excursion (Gorjan et al., 2012; Jones et al., 2016), and both have a chronostratigraphic framework provided by graptolite biostratigraphy (Finney et al., 1997; Chen et al., 2006) (Fig. 2). The Monitor Range section includes the *ornatus* graptolite zone, which precedes the oldest samples from Wangjiawan. The sample sets analyzed here are the same as those described in Jones et al. (2016) for the Monitor Range and in Gorjan et al. (2012) for Wangjiawan.

Carbonate content of whole-rock powders was determined by mass loss following decarbonation with hydrochloric acid. Carbon content of insoluble residue was measured with a Costech ECS 4010 elemental analyzer. The relative standard deviation of TOC measurements was <4.5%. Whole-rock powders were analyzed for Hg with a Teledyne Leeman Labs Hydra II_C mercury analyzer with relative standard deviation <10%.

RESULTS

At Wangjiawan (Fig. 2A), Hg and Hg/TOC rise above background levels in the upper *pacificus* zone, immediately below the first pulse of mass extinction and initiation of shallowing. A second enrichment in Hg begins in shales immediately below the base of the Kuanyinchiao Formation and persists through the shallow-water facies; Hg/TOC reaches ~10× background levels before declining toward baseline just below the Lungamachi Formation.

At the Monitor Range (Fig. 2B), samples with enriched Hg and Hg/TOC occur in the *ornatus* zone in the lower ~60 m of the section. They are succeeded by samples with low background Hg and Hg/TOC through the upper *ornatus* and lower *pacificus* zones. The upper *pacificus* zone is marked by extreme Hg and Hg/TOC enrichments in two limestone samples that reach ~500× background. Based on graptolite and $\delta^{13}C$ chemostratigraphy, the Hirnantian sediment accumulation rate at the Monitor Range is ~80× higher than at Wangjiawan, allowing for sampling at much higher temporal resolution at the Monitor Range. Hirnantian strata contain a series of pulsed Hg anomalies that are ~5–10× higher than the ~6 ppm background.

DISCUSSION

The stratigraphic enrichments in Hg and Hg/TOC may have been controlled by a number of factors, including changes in organic matter

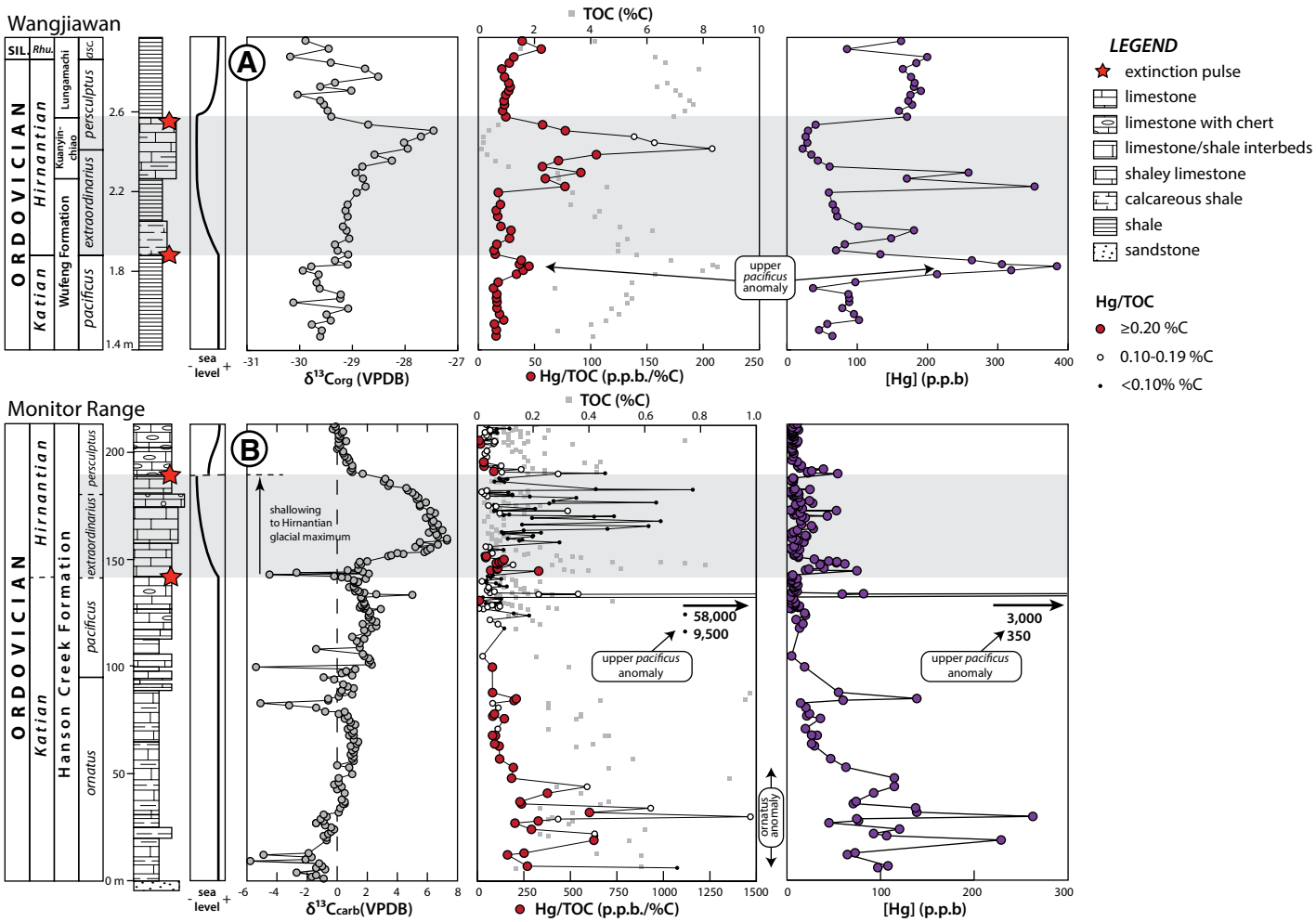

Figure 2. Integrated data for strata deposited across the Late Ordovician mass extinction. SIL—Silurian; Rhu—Rhuddanian; *asc.*—*ascensus*; VPBD—Vienna Peedee belemnite; p.p.b.—parts per billion; TOC—total organic carbon. A: Wangjiawan (south China) lithostratigraphy and graptolite biostratigraphy (Chen et al., 2006), $\delta^{13}C_{org}$ (Gorjan et al., 2012), and Hg chemostratigraphy. B: Monitor Range (western Laurentia; Nevada, USA) lithostratigraphy and graptolite biostratigraphy (Finney et al., 1997), $\delta^{13}C_{carb}$ (Jones et al., 2016), and Hg chemostratigraphy.

content, early diagenetic degradation of organic matter, and enhanced environmental Hg loading. The absence of a strong correlation between Hg and TOC concentrations in the Monitor Range data ($r^2 < 0.01$; Fig. DR1 in the GSA Data Repository[1]) suggests that the stratigraphic pattern of Hg concentration is not solely an artifact of changing TOC content. Although a correlation exists at Wangjiawan, TOC content alone cannot explain all the variability in Hg concentration ($r^2 = 0.53$; Fig. DR1). Because TOC content is commonly lowered during early diagenesis, Hg/TOC ratios have the potential to be diagenetically inflated; this is of particular concern for samples with low TOC. Therefore, we code Hg/TOC data by TOC concentration in Figure 2. The *ornatus* zone Hg/TOC anomaly at the Monitor Range is carried by samples with high (>0.2 wt%) and moderate (0.10–0.20 wt%) TOC content, with concomitant enrichment in absolute Hg concentration (Fig. 2B); these observations support an interpretation of enhanced environmental Hg loading in the latest Katian. The upper *pacificus* zone Hg and Hg/TOC enrichments at both sections differ greatly in magnitude but occur at the same stratigraphic position. At Wangjiawan the upper *pacificus* anomaly is marked by a twofold increase in Hg/TOC and a fourfold increase in Hg concentration above background levels, all in samples with high TOC values (Fig. 2A). Although at the Monitor Range this anomaly is carried by low TOC samples (<0.10 wt% TOC; Fig. 2B), the extreme enrichments in Hg concentration (as high as 500× background levels) are most parsimoniously explained by high environmental fluxes. While a diastem could produce such enrichment, field evidence for a hiatus at this stratigraphic position is lacking (Finney et al., 1997). Hirnantian strata at Wangjiawan contain anomalies in both Hg and Hg/TOC, although the three highest Hg/TOC values are carried by samples with moderate TOC (Fig. 2A). Hirnantian strata at the Monitor Range include samples with Hg concentrations as much as 10× above background levels, suggesting enhanced environmental loading, but low TOC content makes the elevated Hg/TOC values more difficult to interpret.

We argue that the Hg enrichments observed in both sections are the products of enhanced environmental loading caused by LIP emplacement. The sedimentological and stratigraphic context of LIP-generated Hg anomalies may provide insights into Hirnantian glaciation and the LOME. The upper Katian *ornatus* zone anomaly at the Monitor Range (Fig. 2B) is ~1.5–4.0 m.y. older than the start of the Hirnantian (Finney et al., 1997; Sadler et al., 2009). Lefebvre et al. (2010) modeled the consumption of atmospheric CO_2 by emplacement and weathering of a LIP in the late Katian and showed that 5 °C of cooling could occur in 2 m.y., the result being sensitive to the rate, volume, and paleolatitude of LIP emplacement. Our *ornatus* zone Hg data provide indirect geochemical evidence for such a late Katian volcanic event, and we suggest that attendant cooling changed climatic boundary conditions (Finnegan et al., 2011) such that subsequent eruptions had catastrophic effects on climate.

Further LIP emplacement broadly synchronous with the Hirnantian glacial maximum is suggested by Hg records at both sections (Fig. 2). Volcanic SO_2 emission produces sulfur aerosols that can affect climate by increasing planetary albedo upon reaching the stratosphere (Robock, 2000). Global cooling from the weathering of basalt emplaced during an *ornatus* zone eruption would have lowered the tropopause, increasing the likelihood that subsequent eruptions would deliver radiatively active sulfur aerosols to the stratosphere (Macdonald and Wordsworth, 2017). We suggest that rapid expansion of preexisting ice sheets was induced by an albedo catastrophe initiated by a second phase of eruptions represented by the upper *pacificus* zone Hg anomaly. Expanded ice cover was possibly maintained by eruptions throughout the Hirnantian (Fig. 2), facilitated by the positive feedback between cooling and volcanic aerosol injection above the tropopause (Macdonald and Wordsworth, 2017). Because SO_2 must be injected into the stratosphere on a decadal time scale to affect climate (Schmidt et al., 2015), this mechanism would require short hiatuses between eruptions to fully account for the duration of the glacial maximum; estimates for time between flows of the Deccan Traps and Columbia River flood basalts range widely, from 10 to 1000 yr (Self et al., 2014). However, a cascade of environmental change including ice albedo feedback and changes in ocean circulation may have instead maintained the ice extent on longer time scales than the radiative forcing that initiated the ice advance.

Albedo-driven cooling would need to counteract any warming from CO_2 release associated with LIP emplacement, which has been identified as a potential contributor to the Permian-Triassic extinction (e.g., Sun et al., 2012). However, the volume and rate of volcanic CO_2 released during LIP emplacement may be low (Self et al., 2014) and may occur only after an initial phase of SO_2 release due to progressive thermal erosion of the lithosphere (Guex et al., 2016). Furthermore, a critical difference for ice sheet response between the LOME and Permian-Triassic extinction is the existence of a cool climate with preexisting ice cover in the Late Ordovician (Finnegan et al., 2011). Ice expansion at the beginning of the Hirnantian would have been amplified by ice albedo feedback, whereas the warm ocean and continents lacking ice in the late Permian would have hindered the establishment and expansion of ice sheets. Nevertheless, an albedo cooling scenario similar to the one presented here has been proposed for the Permian-Triassic extinction based on high-resolution U/Pb dating of a global marine regression at the boundary and extinction level (Baresel et al., 2017).

Because albedo changes have an instantaneous effect on planetary energy balance, a volcanic trigger could explain the apparent rapidity of the Hirnantian glacial expansion and temperature decline. It may also explain the severity of the first pulse of mass extinction, because marine taxa would have had little opportunity to adapt or migrate to more favorable environments. Late Hirnantian warming from CO_2 release during the later phases of LIP emplacement in concert with a reduction of SO_2 emissions (Guex et al., 2016) may have ultimately caused deglaciation as aerosol albedo forcing waned. The second phase of the LOME is associated with warming, marine transgression, and anoxia (Melchin et al., 2013), all of which are hallmarks of the global environmental effects of LIP-associated CO_2 (Self et al., 2014).

A late Katian–Hirnantian LIP has not yet been identified. However, Ordovician basalts, including the Sierra del Tigre in Argentina (González-Menéndez et al., 2013), the Suordakh in eastern Siberia (Khudoley et al., 2013), and the Cape St. Mary's sills in Newfoundland (Greenough et al., 1993) (Fig. 1A), have loose age constraints that may be compatible with Hirnantian volcanism once they are precisely dated.

CONCLUSION

We document three Hg enrichments associated with the LOME and suggest that they are markers of LIP volcanism. While specific mechanisms linking LIP volcanism to the LOME and Hirnantian glacial maximum are speculative until direct geological and geochronological evidence of a late Katian–Hirnantian LIP is found, the stratigraphic position of the oldest of the Hg anomalies is consistent with modeling predictions linking the chemical weathering of a Katian LIP to Late Ordovician cooling. If the Hg enrichments just preceding the Katian-Hirnantian boundary and through the Hirnantian glacial maximum represent further LIP activity, the synchronous volcanism and glacial expansion may be reconcilable through the albedo effects of volcanic sulfate aerosols. If confirmed, the LIP inferred from our Hg data would join those associated with mass extinction events throughout the Phanerozoic and strengthen the case for LIP volcanism as a primary driver of the environmental changes that caused mass extinction of life on Earth.

[1]GSA Data Repository item 2017205, geochemical data and cross plots, is available online at http://www.geosociety.org/datarepository/2017/ or on request from editing@geosociety.org.

ACKNOWLEDGMENTS

This work was partially funded by Amherst College (Massachusetts, USA). Kaiho was supported by the Japan Society for the Promotion of Science (KAKENHI—Grants-in-Aid for Scientific Research). M. Kopicki and C. Hodge assisted with laboratory work. We thank F. Macdonald and T. Harms for discussions. The manuscript was improved by comments from D. Bond, M. Melchin, and anonymous reviewers.

REFERENCES CITED

Baresel, B., Bucher, H., Bagherpour, B., Brosse, M., Guodun, K., and Schaltegger, U., 2017, Timing of global regression and microbial bloom linked with the Permian-Triassic boundary mass extinction: Implications for driving mechanisms: Scientific Reports, v. 7, 43630, doi:10.1038/srep43630.

Bond, D.P.G., and Wignall, P.B., 2014, Large igneous provinces and mass extinctions: An update, *in* Keller, G., and Kerr, A.C., eds., Volcanism, impacts, and mass extinctions: Causes and effects: Geological Society of America Special Paper 505, p. 29–55, doi:10.1130/2014.2505(02).

Chen, X., Rong, J., Fan, J.-X., Zhan, R., Mitchell, C.E., Harper, D.A.T., Melchin, M.J., Peng, P., Finney, S.C., and Wang, X., 2006, The global boundary stratotype section and point (GSSP) for the base of the Hirnantian Stage (the uppermost of the Ordovician System): Episodes, v. 29, p. 183–196.

Courtillot, V.E., and Renne, P.R., 2003, On the ages of flood basalt events: Comptes Rendus Geoscience, v. 335, p. 113–140, doi:10.1016/S1631-0713(03)00006-3.

Finnegan, S., Bergmann, K., Eiler, J., Jones, D.S., Fike, D.A., Eisenman, I., Hughes, N., Tripati, A., and Fischer, W.W., 2011, The magnitude and duration of Late Ordovician–Early Silurian glaciation: Science, v. 331, p. 903–906, doi:10.1126/science.1200803.

Finney, S.C., Cooper, J.D., and Berry, W.B.N., 1997, Late Ordovician mass extinction: Sedimentologic, cyclostratigraphic, biostratigraphic and chemostratigraphic records from platform and basin successions, central Nevada, *in* Link, P.K., and Kowalis, B.J., eds., Proterozoic to recent stratigraphy, tectonics and volcanology, Utah, Nevada, southern Idaho and central Mexico: Brigham Young University Geology Studies 42, p. 79–103.

Fitzgerald, W.F., Lamborg, C.H., and Hammerschmidt, C.R., 2007, Marine biogeochemical cycling of mercury: Chemical Reviews, v. 107, p. 641–662, doi:10.1021/cr050353m.

Font, E., Adatte, T., Sial, A.N., de Lacerda, L.D., Keller, G., and Punekar, J., 2016, Mercury anomaly, Deccan volcanism, and the end-Cretaceous mass extinction: Geology, v. 44, p. 171–174, doi:10.1130/G37451.1.

González-Menéndez, L., Gallastegui, G., Cuesta, A., Heredia, N., and Rubio-Ordóñez, A., 2013, Petrogenesis of early Paleozoic basalts and gabbros in the western Cuyania terrane: Constraints on the tectonic setting of the southwestern Gondwana margin (Sierra del Tigre, Andean Argentine Precordillera): Gondwana Research, v. 24, p. 359–376, doi:10.1016/j.gr.2012.09.011.

Gorjan, P., Kaiho, K., Fike, D.A., and Xu, C., 2012, Carbon- and sulfur-isotope geochemistry of the Hirnantian (Late Ordovician) Wangjiawan (Riverside) section, south China: Global correlation and environmental event interpretation: Palaeogeography, Palaeoclimatology, Palaeoecology, v. 337–338, p. 14–22, doi:10.1016/j.palaeo.2012.03.021.

Greenough, J.D., Kamo, S.L., and Krogh, T.E., 1993, A Silurian U-Pb age for the Cape St. Mary's sills, Avalon Peninsula, Newfoundland, Canada: Implications for Silurian orogenesis in the Avalon Zone: Canadian Journal of Earth Sciences, v. 30, p. 1607–1612, doi:10.1139/e93-138.

Guex, J., Pilet, S., Müntener, O., Bartolini, A., Spangenberg, J., Schoene, B., Sell, B., and Schaltegger, U., 2016, Thermal erosion of cratonic lithosphere as a potential trigger for mass-extinction: Scientific Reports, v. 6, 23168, doi:10.1038/srep23168.

Herrmann, A.D., Haupt, B., Patzkowsky, M., Seidov, D., and Slingerland, R.L., 2004, Response of Late Ordovician paleoceanography to changes in sea level, continental drift, and atmospheric pCO_2: Potential causes for long-term cooling and glaciation: Palaeogeography, Palaeoclimatology, Palaeoecology, v. 210, p. 385–401, doi:10.1016/j.palaeo.2004.02.034.

Jones, D.S., Creel, R.C., and Rios, B.A., 2016, Carbon isotope stratigraphy and correlation of depositional sequences in the Upper Ordovician Ely Springs Dolostone, eastern Great Basin, USA: Palaeogeography, Palaeoclimatology, Palaeoecology, v. 458, p. 85–101, doi:10.1016/j.palaeo.2016.01.036.

Khudoley, A.K., Prokopiev, A.V., Chamberlain, K.R., Ernst, R.E., Jowitt, S.M., Malyshev, S.V., Zaitsev, A.I., Kropachev, A.P., and Koroleva, O.V., 2013, Early Paleozoic mafic magmatic events on the eastern margin of the Siberian craton: Lithos, v. 174, p. 44–56, doi:10.1016/j.lithos.2012.08.008.

Kilian, T.M., Swanson-Hysell, N.L., Bold, U., Crowley, J.L., and Macdonald, F.A., 2016, Paleomagnetism of the Teel basalts from the Zavkhan terrane: Implications for Paleozoic paleogeography in Mongolia and the growth of continental crust: Lithosphere, v. 8, p. 699–715, doi:10.1130/L552.1.

Lefebvre, V., Servais, T., François, L., and Averbuch, O., 2010, Did a Katian large igneous province trigger the Late Ordovician glaciation?: Palaeogeography, Palaeoclimatology, Palaeoecology, v. 296, p. 310–319, doi:10.1016/j.palaeo.2010.04.010.

Macdonald, F.A., and Wordsworth, R., 2017, Initiation of Snowball Earth with volcanic sulfur aerosol emissions: Geophysical Research Letters, v. 278, p. 1–9, doi:10.1029/2001JD002042.

Melchin, M.J., Mitchell, C.E., Holmden, C., and Štorch, P., 2013, Environmental changes in the Late Ordovician–Early Silurian: Review and new insights from black shales and nitrogen isotopes: Geological Society of America Bulletin, v. 125, p. 1635–1670, doi:10.1130/B30812.1.

Pohl, A., Donnadieu, Y., Le Hir, G., Ladant, J.B., and Dumas, C., 2016, Glacial onset predated Late Ordovician climate cooling: Paleoceanography, v. 31, doi:10.1002–2016PA002928.

Robock, A., 2000, Volcanic eruptions and climate: Reviews of Geophysics, v. 38, p. 191–219, doi:10.1029/1998RG000054.

Sadler, P.M., Cooper, R.A., and Melchin, M., 2009, High-resolution, early Paleozoic (Ordovician–Silurian) time scales: Geological Society of America Bulletin, v. 121, p. 887–906, doi:10.1130/B26357.1.

Saltzman, M.R., and Young, S.A., 2005, Long-lived glaciation in the Late Ordovician? Isotopic and sequence-stratigraphic evidence from western Laurentia: Geology, v. 33, p. 109–112, doi:10.1130/G21219.1.

Sanei, H., Grasby, S.E., and Beauchamp, B., 2012, Latest Permian mercury anomalies: Geology, v. 40, p. 63–66, doi:10.1130/G32596.1.

Schmidt, A., et al., 2015, Selective environmental stress from sulphur emitted by continental flood basalt eruptions: Nature Geoscience, v. 9, p. 77–82, doi:10.1038/ngeo2588.

Schuster, P.F., Krabbenhoft, D.P., Naftz, D.L., Cecil, L.D., Olson, M.L., Dewild, J.F., Susong, D.D., Green, J.R., and Abbott, M.L., 2002, Atmospheric mercury deposition during the last 270 years: A glacial ice core record of natural and anthropogenic sources: Environmental Science & Technology, v. 36, p. 2303–2310, doi:10.1021/es0157503.

Self, S., Schmidt, A., and Mather, T.A., 2014, Emplacement characteristics, time scales, and volcanic gas release rates of continental flood basalt eruptions on Earth, *in* Keller, G., and Kerr, A.C., eds., Volcanism, impacts, and mass extinctions: Causes and effects: Geological Society of America Special Paper 505, p. 319–337, doi:10.1130/2014.2505(16).

Selin, N.E., 2009, Global biogeochemical cycling of mercury: A review: Annual Review of Environment and Resources, v. 34, p. 43–63, doi:10.1146/annurev.environ.051308.084314.

Sun, Y., Joachimski, M.M., Wignall, P.B., Yan, C., Chen, Y., Jiang, H., Wang, L., and Lai, X., 2012, Lethally hot temperatures during the Early Triassic greenhouse: Science, v. 338, p. 366–370, doi:10.1126/science.1224126.

Thibodeau, A.M., Ritterbush, K., Yager, J.A., West, A.J., Ibarra, Y., Bottjer, D.J., Berelson, W.M., Bergquist, B.A., and Corsetti, F.A., 2016, Mercury anomalies and the timing of biotic recovery following the end-Triassic mass extinction: Nature Communications, v. 7, 11147, doi:10.1038/ncomms11147.

Trotter, J.A., Williams, I.S., Barnes, C.R., Lécuyer, C., and Nicoll, R.S., 2008, Did cooling oceans trigger Ordovician biodiversification? Evidence from conodont thermometry: Science, v. 321, p. 550–554, doi:10.1126/science.1155814.

Manuscript received 5 January 2017
Revised manuscript received 15 March 2017
Manuscript accepted 16 March 2017

Printed in USA